

Cite this: *J. Mater. Chem.*, 2012, **22**, 18115

www.rsc.org/materials

MnO₂/graphene oxide: a highly active catalyst for amide synthesis from alcohols and ammonia in aqueous media†Renfeng Nie,^a Juanjuan Shi,^a Shuixin Xia,^a Lian Shen,^b Ping Chen,^a Zhaoyin Hou^{*a} and Feng-Shou Xiao^a

Received 16th July 2012, Accepted 31st July 2012

DOI: 10.1039/c2jm34652d

Rod-like MnO₂ uniformly attached on both side of GO sheets (MnO₂/GO) is an efficient heterogeneous catalyst for the synthesis of primary amides from primary alcohols and ammonia as well as from aldehydes or nitriles. Water is the best solvent for these reactions, analytically pure crystals of product could be isolated by simply cooling in ice and this catalyst has excellent recyclability.

Amide is one of the most important functional groups and plays a major role in the elaboration and composition of biological as well as chemicals and polymer compounds,^{1–5} while the formation of amide bonds remains a challenge in organic synthesis.^{2,6} The most traditional method for amide synthesis is from activated carboxylic acid derivatives, such as acids,⁶ aldehydes,^{7,8} acyl halides,⁹ ketones or carbinols,¹⁰ mixed anhydrides¹¹ and esters which react with amines or acyl azides,¹² and/or from the reactions of acyl hydrazides with reductants.^{13,14} Alternative procedures include the hydration of nitriles to primary amides in the presence of acids,¹⁵ bases,¹⁶ or transition metal catalysts including homogeneous^{17,18} and heterogeneous complexes.¹⁹ Other methods such as Beckmann rearrangement, Aube–Schmidt rearrangement, and Staudinger reaction are also commonly reported in published papers.^{20–23} However, limitations in existing methods, such as the use of toxic inorganic cyanides or production of vast amounts of wasteful inorganic salts, severely hinder their application for amide synthesis at a large scale in industrial processes.^{24–27}

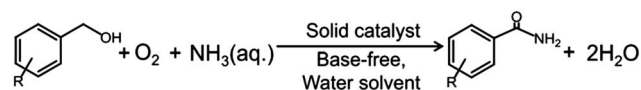
Recently, heterogeneous catalysts for direct synthesis of amides from primary alcohols and amines have been paid much attention due to their high efficiency, easy catalyst recycling, and high atomic economy. Shimizu *et al.* reported an oxidant-free dehydrogenative amide synthesis from primary alcohols and secondary amines over Ag/Al₂O₃ catalyst, in which toluene was selected as solvent and excessive base was added.²⁷ Wang and co-workers disclosed an Au/DNA catalyst for the formation of secondary amides from alcohols and amines using LiOH·H₂O as a base promoter.²⁸ Ruthenium-based catalysts were also widely used for syntheses of

amides from alcohols, aldehydes with NH₃ or nitriles.^{16,29,30} More recently, Yamaguchi *et al.* found that OMS-2 can also catalyze the synthesis of primary amides from alcohols (or aldehydes) and aqueous ammonia using 1,4-dioxane as a solvent.^{31,32}

However, there still remains a challenge for the improvement of these reported methods, because the preparations of catalysts are time-consuming and precious metals have relatively high cost and these reactions require the use of organic solvents. Therefore, amide synthesis from alcohols and ammonia in a green solvent—water—over a cheap and active heterogeneous catalyst is strongly desirable (Scheme 1).

MnO₂ is a cheap, low toxic, easily handled reagent,³³ which has been used as catalyst in alcohol oxidations under mild conditions for a long time.^{31–37} However, MnO₂ usually delivers a relatively low surface area (10–80 m² g⁻¹) and limited electrical conductivity,³⁸ which strongly depresses its catalytic activities. It is well known that graphene oxide (GO) possesses large surface area (up to 400–1500 m² g⁻¹)^{39,40} because both sides of the nanosheets are accessible.⁴¹ The functionalities of surface groups^{40,42,43} and the presence of holes,⁴⁴ oxygen,⁴⁵ carbon vacancies and defects, which are generated in partial oxidation produced sheets from graphitic domains,^{46,47} may introduce chemically active sites in catalysis and also act as anchoring sites for deposition of metal nanoparticles. It has been suggested that GO could be an ideal support for growth of functional nanoparticles and would render them electrically conductive, highly dispersive, and catalytically active.³⁹

Herein, by combining the advantages of MnO₂ nanocrystals (active catalyst) with GO (large surface area, good electrical conductivity and outstanding dispersion in water medium), an effective and fast one-pot soft chemical route has been adopted to directly produce a well-organized MnO₂ nanorods/graphene oxide composite (MnO₂/GO). This hybrid material was first used as a new efficient and recyclable heterogeneous catalyst in the direct synthesis of amides from primary alcohols and aqueous ammonia in the presence of a green solvent (water). Very importantly, catalyst/product separation is easy because of the green solvent water, and this catalyst is active compared with conventional manganese catalysts.



Scheme 1 Green and atom-economical synthesis of primary amides.

^aInstitute of Catalysis, Department of Chemistry, Zhejiang University, 310028 Hangzhou, P. R. China. E-mail: zyhoul@zju.edu.cn; Fax: +86 571 88273283; Tel: +86 571 88273283

^bCollege of Chemical Engineering and Materials Science, Zhejiang University of Technology, 310014 Hangzhou, P. R. China

† Electronic supplementary information (ESI) available. See DOI: 10.1039/c2jm34652d

Fig. S1 (ESI†) shows X-ray diffraction (XRD) patterns of GO, MnO₂, and MnO₂/GO. The (002) diffraction peak of GO in MnO₂/GO (Fig. S1a†) shifted slightly to a high angle around 11.6° with nearly the same basal spacing of 0.87 nm but lower intensity than that of pure GO (Fig. S1b†). These results suggest that the presence of more disordered stacking, less agglomeration of GO sheets in the composite and the regular stacks of GO are exfoliated continuously due to the insert of MnO₂ nanoparticles.^{48,49} The diffraction peaks of α -MnO₂ (JCPDS 44-0141) in MnO₂/GO are faint, compared with bare MnO₂, which indicates that MnO₂ nanoparticles deposited on GO are in small sizes. On the other hand, free MnO₂ prepared *via* a similar approach shows strong diffraction peaks (Fig. S1c†), which implies a good degree of crystallization or the presence of larger nanocrystallites (Fig. S2a†).⁵⁰ Fig. S3† shows N₂ adsorption isotherms of MnO₂ and MnO₂/GO. Obviously, MnO₂/GO (112 m² g⁻¹, 0.613 cm³ g⁻¹) exhibits much higher surface area as well as pore volume than MnO₂ (79 m² g⁻¹, 0.307 cm³ g⁻¹). Correspondingly, MnO₂/GO shows major mesopores centered at 35.0 nm, much larger than that of MnO₂ (14.9 nm average pore diameter). These improvements in hierarchical porous structure (including mesopores and macropores) and larger surface area can improve the contact between active sites with the substrate in reaction solution.

Fig. S4† shows the Raman spectra of GO, MnO₂, and MnO₂/GO. Notably, MnO₂/GO exhibits characteristics of both GO and MnO₂.⁵¹ The bands at 500–700 cm⁻¹ can be assigned to A_g spectroscopic species that originate from breathing vibrations of MnO₆ octahedra within a tetragonal hollandite-type framework, whereas the low-frequency bands at 200–400 cm⁻¹ are assigned to the bending modes of Mn–O.⁵² The calculated I_D/I_G intensity ratio of MnO₂/GO (1.06) is higher than that of GO (0.91), indicating the growth of *in situ* formed crystals may also in turn contribute to the destruction of regular layered GO sheets and the formation of exfoliated graphene oxide.⁵¹ Fig. S5† shows XPS spectra of GO, MnO₂, and MnO₂/GO. Deconvolution of the C1s peak (Fig. S5a†) reveals the presence of 38.6% heterocarbon, which is slightly lower than that of GO (48.2%) (Fig. S5b, Table S1†), in agreement with XRD and Raman analyses. The decreased oxygen-containing groups (C–O and C=O) are expected to capture Mn²⁺ ions, partially reduced by Mn²⁺ ions and anchored MnO₂ nanoparticles on the surface of GO. The O1s spectrum of MnO₂/GO shows two peaks, in comparison with that of GO. The dominant peak at 529.6 eV is assigned to the oxygen bonded with manganese (Mn–O) in MnO₂ (Fig. S5c†), and another O1s peak at 532.1 eV might be attributed to oxygen-containing groups of GO.^{45,53} The Mn2p spectrum exhibits two characteristic peaks at 641.9 and 653.6 eV, corresponding to Mn2p_{3/2} and Mn2p_{1/2} spin orbit peaks of α -MnO₂ (Fig. S5d†).^{45,54} These results indicate that the *in situ* growth of MnO₂ crystals can render MnO₂/GO conductive *via* electron transfer. At the same time, the functional groups of GO sheets would improve its dispersion in aqueous media (Fig. S6†).

Fig. 1 shows transmission electron microscopic (TEM) images of MnO₂/GO nanocomposites obtained from various time intervals. Pure GO sheet is a transparent film (Fig. S2b†), crumpling and agglomeration exists throughout the sheet, as a result of deformation upon the exfoliation and restacking process. After addition of manganese salts in the starting system, rare needle-like MnO₂ with diameters of 3–10 nm and lengths of 20–500 nm were dispersed randomly on the surface of GO in short refluxing time (15 min, Fig. 1a). The amount of MnO₂ nanoneedles formed on the surface of

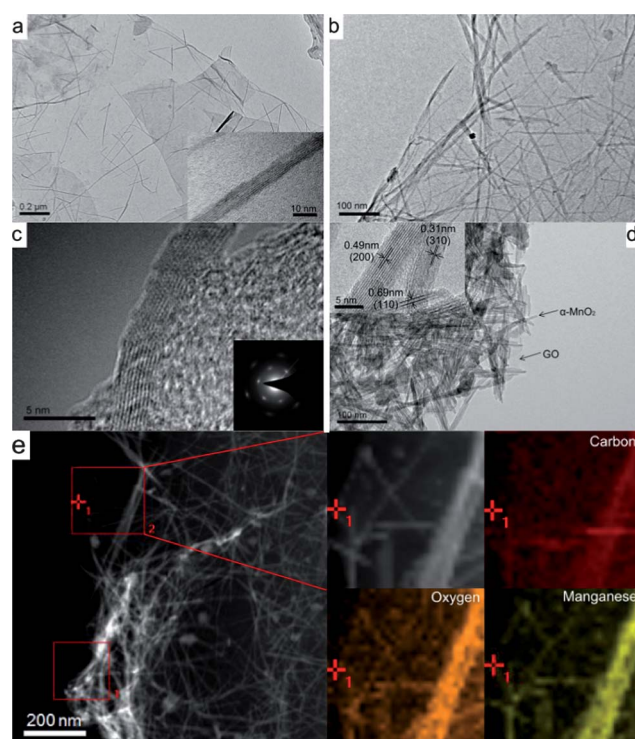


Fig. 1 TEM images of MnO₂/GO nanocomposites obtained at different time intervals of (a) 15 (inset: HRTEM image), (b) 60 min, (c) 60 min (HRTEM image, inset: SAED pattern), (d) 120 min (inset: HRTEM image), and (e) STEM images and EDX of C, O, Mn of in sample d.

GO increased continuously with increasing refluxing time (from 15 to 60 min) *via* a dissolution–crystallization mechanism,⁵¹ which finally gives rise to wider MnO₂ nanoneedles on GO sheets (Fig. 1b). All diffraction spots in the SAED pattern of MnO₂/GO (Fig. 1c) could be indexed as a body-centered tetragonal phase, indicating that MnO₂ nanoneedles are single crystals. The morphology of MnO₂ changed gradually from needle-like to rod-like (5–20 nm in diameter) through aggregating along the lateral faces when the refluxing time was prolonged to 120 min (Fig. 1d). These rod-like MnO₂ were uniformly and densely attached on both sides of GO, leading to thick and dense nanohybrid sheets. In addition, SEM images also suggest MnO₂ nanorods were highly dispersed on the GO sheets (Fig. S2†). These results indicated that the size of MnO₂ nanorods could be controlled *via* manipulating the refluxing time. HRTEM images of MnO₂/GO obtained at a refluxing time of 120 min (Fig. 1d) clearly show the lattice fringes with *d* spacings of 0.31, 0.49 and 0.69 nm, corresponding to the (310), (200) and (110) planes of α -MnO₂ crystals, respectively. STEM image and EDX analysis (Fig. 1e) show that there is a good spatial correspondence of C, O and Mn elemental maps. It was found that the assembly of nanorods on the surface of graphene sheets to some extent prevents the stacking of GO sheets due to van der Waals interactions, leading to a large available surface area and rich porous structure for transferring reactants and products. On the other hand, SEM and TEM revealed smaller diameters in MnO₂/GO (~5–20 nm in diameter, Fig. 1d) than bare MnO₂ (~20–40 nm in diameter, Fig. S2a†). These results fit well with the theoretical predictions that the graphene sheets could isolate the growth of metal nanowires.^{55,56}

The catalytic performance of MnO₂/GO for the transformation of benzyl alcohol with molecular O₂ and aqueous ammonia (28%) to benzamide in various solvents is presented in Table S2.† Clearly, 1,4-dioxane, DMF and DMSO are good solvents for this reaction, but yields of benzamide were relatively low (<25%, entries 2–4). When water was employed as a solvent, the yield of benzamide reached 58.5% at 1 h (entry 1), and further increased to 97% at 3 h (entry 11, Table S2†). This yield is comparable to that of OMS-2 in 1,4-dioxane solvent.^{31,32} Noble metal catalysts are active for the oxidation of alcohols (aldehydes), but require assistance from supports or bases for nitrile hydration step.^{16,29,30}

It seems that an excess amount of water is beneficial for the hydration of nitriles to the corresponding amides, and a large amount of oxygen-containing groups on GO sheets can improve the dispersion of the MnO₂/GO catalyst in aqueous media (Fig. S6†), which provides a sufficient contact between active sites of MnO₂ nanorods and the substrate. The MnO₂/GO catalyst could be easily separated from the reaction mixture by filtration (Fig. S7a and b†). After separation of the catalyst, analytically pure white crystals of benzamide appeared when the filtrate was cooled in ice (Fig. S7c†). These crystals could be easily isolated by filtration with high yield (>80%).

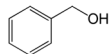
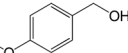
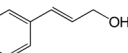
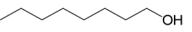
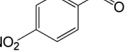
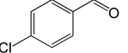
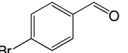
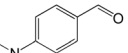
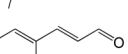
In contrast, this reaction does not work in the absence of catalysts (entry 10, Table S2†); MnO₂ (prepared *via* a similar procedure as MnO₂/GO, entry 7), MnCl₂ (entry 8) and GO (entry 9) also show relatively low activities (yield of benzamide <10%). These results suggested that the size of MnO₂ nanorods plays a crucial role in the catalytic activity, and the enhanced activity of MnO₂/GO could be attributed to its high dispersion in water, high MnO₂ dispersion on GO and suitable functional groups on carbon materials.

In order to verify whether the observed catalysis is truly heterogeneous, the reaction was stopped after 0.5 h by filtering MnO₂/GO from the reaction mixture, and then heated again for 3 h, but no further production of benzamide was observed. This result suggested that the observed catalysis is truly heterogeneous in nature. Moreover, after five recycles, MnO₂/GO still shows high TOF mol (mol_{Mn} h)⁻¹ relative to the initial TOF of 0.15 (Fig. S8†), indicating that MnO₂/GO nanohybrid is really recyclable.

Importantly, when various primary alcohols or aldehydes are used as substrates, MnO₂/GO nanohybrid catalyst still gives very high activities and yields (Table 1). In the transformation of benzylic alcohols (aldehydes) to the corresponding amides (entries 2, 6–9), the catalyst has high yields (>93% yields) toward electron-donating as well as electron-withdrawing substituents, whereas weak electronegativity such as Br has a negative influence on this reaction (entry 8). Additionally, allylic alcohols or aldehydes proceeded efficiently to afford the corresponding unsaturated amides without isomerization and hydrogenation of the double bond (entries 3 and 10). Aliphatic alcohol could also be converted to the corresponding amide in slightly lower yield (entry 4).

Fig. S9† shows catalytic kinetics for the conversion of benzyl alcohol, benzyl aldehyde, and benzonitrile to benzamide over MnO₂/GO. When benzyl alcohol was used as a reactant, it was observed that benzyl aldehyde, benzonitrile, and benzamide formed consecutively (Fig. S9a†). After reaction for 1 h, benzyl alcohol was almost consumed, benzonitrile reached its maximum yield (>35% yield). The yield of benzamide increased steadily with reaction time (0–3 h). For benzyl aldehyde (Fig. S9b†), it was found that benzyl aldehyde was converted completely within 15 min. The yield of benzonitrile reached its maximum (78%) at 15 min, and then decreased continuously with

Table 1 Conversion and yield of amides from primary alcohols (aldehydes) and ammonia^a

Entry	Substrate	Time (h)	Conversion (%)	Yield (%)
1		3	100	97.0
2		3	100	96.5
3 ^b		5	100	98.0
4		30	93.5	61.5
5		3	100	97.9
6		3	100	97.4
7		3	100	97.2
8		3	98.7	93.8
9		5	100	96.3
10 ^b		5	100	98.4

^a Reaction conditions: substrate (0.5 mmol), MnO₂/GO (0.13 g), 28% aq. ammonia (0.1 mL), water (4 mL), O₂ (3 MPa), 150 °C. ^b 130 °C.

the steadily increased yield of benzamide. On the other hand, benzamide formed slowly with increasing reaction time when benzonitrile was used as a reactant (Fig. S9c†). These results suggest that the dehydration of aldehyde goes faster than the hydration of nitrile to amide.

According to these results, it could be deduced that a route from alcohol to amide follows a sequential transformation: benzyl alcohol → benzyl aldehyde → benzonitrile → benzamide (Fig. 2). The rate constant of each step could be calculated from the linear regression between reaction time (*t*) and ln(*n*₀/*n*₀ - *n*) plot as the slope of plus one. It was concluded that the rate constant of dehydration of aldehyde (*k*₂ = 12.9 h⁻¹) is faster than the oxidative dehydrogenation of alcohol (*k*₁ = 3.13 h⁻¹), and hydration of benzonitrile (*k*₃ = 1.07 h⁻¹) goes slower than the previous two steps. That is, hydration of benzonitrile is the rate-determining step in the transformation of benzyl alcohol to benzamide in aqueous solution over MnO₂/GO

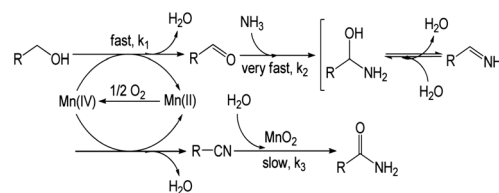


Fig. 2 Possible reaction pathway of amidation from primary alcohols to primary amides catalyzed by MnO₂/GO.

catalyst. These results are consistent with the suggestion that an excess of water is beneficial for the hydration of nitriles to the corresponding amides and water is a superior medium for the direct synthesis of amides from primary alcohols (Table S2†).

In summary, well-organized MnO₂ nanorods on graphene oxide (MnO₂/GO) were fabricated through a novel and easily controlled chemical route. Rod-like MnO₂ with 5–20 nm diameter and 100–600 nm length were uniformly and densely attached on both side of GO sheets. Compared with bare MnO₂, the MnO₂/GO nanocomposite is an efficient heterogeneous catalyst for a widely applicable synthesis of primary amides from primary alcohols and ammonia as well as for transformation of aldehydes or nitriles. More importantly, water is a superior medium for this reaction compared with other commonly used organic solvents, which is beneficial for catalyst/product separation. MnO₂/GO catalyst has good recyclability in these reactions. High dispersion in water, high MnO₂ dispersion on GO and suitable functional groups on carbon materials are important for a synergistic ammoxidation catalytic activity of MnO₂ and GO in the hybrid. These features should be potentially important for the synthesis of fine chemicals and pharmaceuticals in the future.

Acknowledgements

This work was financially supported by the National Natural Science Foundation of China (Contract nos. 21073159, LZ12B030001).

Notes and references

- 1 C. L. Allen and J. M. Williams, *Chem. Soc. Rev.*, 2011, **40**, 3405.
- 2 E. Valeur and M. Bradley, *Chem. Soc. Rev.*, 2009, **38**, 606.
- 3 S. A. Lawrence, *Amines: Synthesis, Properties and Applications*, Cambridge University Press, Cambridge, 2005.
- 4 C. Gunanathan and D. Milstein, *Angew. Chem., Int. Ed.*, 2008, **47**, 8661.
- 5 B. Schlummer and U. Scholz, *Adv. Synth. Catal.*, 2004, **346**, 1599.
- 6 V. R. Pattabiraman and J. W. Bode, *Nature*, 2011, **480**, 471.
- 7 A. Khalafi-Nezhad, A. Parhami, M. N. S. Rad and A. Zarea, *Tetrahedron Lett.*, 2005, **46**, 6879.
- 8 W. J. Yoo and C. J. Li, *J. Am. Chem. Soc.*, 2006, **128**, 13064.
- 9 R. Ohmura, M. Takahata and H. Togo, *Tetrahedron Lett.*, 2010, **51**, 4378.
- 10 L. P. Cao, J. Y. Ding, M. Gao, Z. H. Wang, J. Li and A. X. Wu, *Org. Lett.*, 2009, **11**, 3810.
- 11 M. Mentel, M. J. Beier and R. Breinbauer, *Synthesis*, 2009, **9**, 1463.
- 12 G. E. Veitch, K. L. Bridgwood and S. V. Ley, *Org. Lett.*, 2008, **10**, 3623.
- 13 M. B. Smith, *Compendium of Organic Synthetic Methods*, Wiley, New York, 2001.
- 14 B. Shen, D. M. Makley and J. N. Johnston, *Nature*, 2010, **465**, 1027.
- 15 M. Tamura, H. Wakasugi, K. Shimizu and A. Satsuma, *Chem.–Eur. J.*, 2011, **17**, 11428.
- 16 K. Yamaguchi, M. Matsushita and N. Mizuno, *Angew. Chem., Int. Ed.*, 2004, **43**, 1576.
- 17 K. Yamaguchi, H. Fujiwara, Y. Ogasawara, M. Kotani and N. Mizuno, *Angew. Chem.*, 2007, **119**, 3996.
- 18 T. Zweifel, J. V. Naubron and H. Grützmacher, *Angew. Chem., Int. Ed.*, 2009, **48**, 559.
- 19 M. G. Crestani, A. Arévalo and J. J. García, *Adv. Synth. Catal.*, 2006, **348**, 732.
- 20 F. Damkaci and P. DeShong, *J. Am. Chem. Soc.*, 2003, **125**, 4408.
- 21 K. Tani and B. M. Stoltz, *Nature*, 2006, **441**, 731.
- 22 N. A. Owston, A. J. Parker and J. M. J. Williams, *Org. Lett.*, 2007, **9**, 3599.
- 23 C. Chen and S. H. Hong, *Org. Biomol. Chem.*, 2011, **9**, 20.
- 24 P. T. Anastas and J. C. Warner, *Green Chemistry: Theory and Practice*, Oxford University Press, Oxford, 1998.
- 25 J. H. Clark, *Green Chem.*, 1999, **1**, 1.
- 26 Thematic issue on “Green Chemistry”, *Acc. Chem. Res.*, 2002, **35**, 685.
- 27 K. Shimizu, K. Ohshima and A. Satsuma, *Chem.–Eur. J.*, 2009, **15**, 9977.
- 28 Y. Wang, D. P. Zhu, L. Tang, S. J. Wang and Z. Y. Wang, *Angew. Chem., Int. Ed.*, 2011, **50**, 8917.
- 29 T. Oishi, K. Yamaguchi and N. Mizuno, *Angew. Chem., Int. Ed.*, 2009, **48**, 6286.
- 30 T. Oishi, K. Yamaguchi and N. Mizuno, *Top. Catal.*, 2010, **53**, 479.
- 31 K. Yamaguchi, H. Kobayashi, T. Oishi and N. Mizuno, *Angew. Chem., Int. Ed.*, 2011, **50**, 1.
- 32 K. Yamaguchi, H. Kobayashi, Y. Wang, T. Oishi, Y. Ogasawara and N. Mizuno, *Catal. Sci. Technol.*, 2013, DOI: 10.1039/c2cy20178j.
- 33 X. C. Yu, C. Z. Liu, L. Jiang and Q. Xu, *Org. Lett.*, 2011, **13**, 6184.
- 34 V. D. Makwana, Y. C. Son, A. R. Howell and S. L. Suib, *J. Catal.*, 2002, **210**, 46.
- 35 Y. Wang, H. Kobayashi, K. Yamaguchi and N. Mizuno, *Chem. Commun.*, 2012, **48**, 2642.
- 36 X. J. Yang, J. Y. Han, Z. P. Du, H. Yuan, F. Jin and Y. X. Wu, *Catal. Commun.*, 2010, **11**, 643.
- 37 T. Oishi, K. Yamaguchi and N. Mizuno, *ACS Catal.*, 2011, **1**, 1351.
- 38 V. B. R. Boppana and F. Jiao, *Chem. Commun.*, 2011, **47**, 8973.
- 39 D. Li and R. B. Kaner, *Science*, 2008, **320**, 1170.
- 40 G. M. Scheuermann, L. Rumi, P. Steurer, W. Bannwarth and R. Mülhaupt, *J. Am. Chem. Soc.*, 2009, **131**, 8262.
- 41 R. F. Nie, J. H. Wang, L. N. Wang, Y. Qin, P. Chen and Z. Y. Hou, *Carbon*, 2012, **50**, 586.
- 42 Y. J. Gao, D. Ma, L. Wang, J. Guan and X. H. Bao, *Chem. Commun.*, 2011, **47**, 2432.
- 43 Z. P. Zhu, D. S. Su, G. Weinberg and R. Schlögl, *Nano Lett.*, 2004, **4**, 2255.
- 44 K. Erickson, R. Erni, Z. H. Lee, N. Alem, W. Gannett and A. Zettl, *Adv. Mater.*, 2010, **22**, 4467.
- 45 R. I. Jafri, N. Rajalakshmi and S. Ramaprabhu, *J. Mater. Chem.*, 2010, **20**, 7114.
- 46 Y. Li, X. B. Fan, J. J. Qi, J. Y. Ji, S. L. Wang, G. L. Zhang and F. B. Zhang, *Nano Res.*, 2010, **3**, 429.
- 47 E. J. Yoo, T. Okata, T. Akita, M. Kohyama, J. Nakamura and I. Honma, *Nano Lett.*, 2009, **9**, 2255.
- 48 M. N. Patel, X. Q. Wang, D. A. Slanac, D. A. Ferrer, S. Dai, K. P. Johnston and K. J. Stevenson, *J. Mater. Chem.*, 2012, **22**, 3160.
- 49 J. Su, M. H. Cao, L. Ren and C. W. Hu, *J. Phys. Chem. C*, 2011, **115**, 14469.
- 50 H. J. Huang and X. Wang, *Nanoscale*, 2011, **3**, 3185.
- 51 S. Chen, J. W. Zhu, X. D. Wu, Q. F. Han and X. Wang, *Nano*, 2010, **4**, 2822.
- 52 T. Gao, H. Fjellvåg and P. Norby, *Anal. Chim. Acta*, 2009, **648**, 235.
- 53 H. W. Nesbitt and D. Banerjee, *Am. Mineral.*, 1998, **83**, 305.
- 54 D. Banerjee and H. W. Nesbitt, *Geochim. Cosmochim. Acta*, 2001, **65**, 1703.
- 55 Y. F. Li, H. Q. Yu, H. Li, C. G. An, K. Zhang, K. M. Liew and X. F. Liu, *J. Phys. Chem. C*, 2011, **115**, 6229.
- 56 Y. F. Li, H. Li, K. Zhang and K. M. Liew, *Carbon*, 2012, **50**, 566.